Geophys. J. Int. (2001) **146,** 282–288

Seismic evidence for a mantle plume oceanwards of the Kamchatka–Aleutian trench junction

A. Gorbatov,[1,*] Y. Fukao,[1] S. Widiyantoro[1,†] and E. Gordeev[2]

[1] *Earthquake Research Institute, University of Tokyo, Yayoi* 1-1-1, *Bunkyo-ku, Tokyo* 113–0032, *Japan. E-mail:alexei.gorbatov.anu.edu.au*
[2] *Geophysical Survey of Russia, Piip Avenue* 9, *Petropavlovsk-Kamchatsky,* 683006, *Russia*

Accepted 2001 February 8. Received 2000 November 13; in original form 1999 December 15

SUMMARY

A non-linear iterative *P*-wave traveltime tomography has revealed a mantle plume originating at a depth of nearly 1000 km, rising across the 600 km discontinuity, and deflecting subhorizontally in the uppermost mantle presumably by shear flow due to the overlying moving plate. Data from the Geophysical Survey of Russia (1955–1997) were inverted jointly with the catalogues of International Seismological Centre and USGS National Earthquake Information Centre (1964– 1998). The result shows a 300–500 km-wide cylindrical low-velocity anomaly (~ -2 per cent) that extends from a depth of greater than 900 km to shallower than 200 km. The anomaly is almost vertical at depths up to $\sim$400 km and rises obliquely to the north up to $\sim$200 km under the ocean floor near the northern end of Emperor seamounts. Above $\sim$300 km depth a subsidiary anomaly extends subhorizontally to the NW in fair agreement with the direction of movement of the Pacific Plate. The overlying seafloor is characterized by anomalously high heat flow, which may be attributed to the thermal effect of the mantle plume.

Key words: heat flow, Kamchatka–Aleutian trench, mantle plume, Pacific Plate, transition zone.

INTRODUCTION

The Kamchatka subduction zone is one of the most active seismic regions of the world (Fig. 1). The old Pacific plate subducts below the North American Plate, causing high seismic and volcanic activities in the region. The maximum depth of seismicity changes gradually from $\sim$600 km to $\sim$300 km with latitude increasing from $\sim$50°N to $\sim$54°N. Then, it decreases sharply to a depth of $\sim$100 km further to the north. Hypocentral distribution shows that the dip of the descending slab remains constant in a latitudinal range from $\sim$50°N to $\sim$54°N but is anomalously shallow between $\sim$54°N and $\sim$56°N (Gorbatov *et al.* 1997). As in other regions, the sharp change in the subduction geometry across $\sim$54°N is well reflected in the geometry of the volcanic arc. The maximum depth and dip angle of seismicity to the south of $\sim$54°N are typical for subduction of the Pacific Plate of Cretaceous age, while those to the north are unusual in the sense that they are characteristic of subduction of a plate with a thermal age two to three times younger (Gorbatov *et al.* 1997). In contrast, there is no sharp variation of age on the Pacific seafloor along the Kamchatka Trench (Renkin & Sclater 1988; Rea *et al.* 1993). The ocean floor in the relevant region is marked by Meiji Guyot, a large seamount at the northern end of the Emperor seamount chain as shown in Fig. 1. As will be discussed later, the topographic and gravimetric features of Meiji Guyot are quite different from those of the seamounts further to the south. The heat flow is anomalously high (more than 80 mW m^{-2}) compared to the adjacent oceanic floor, suggesting a reduced thermal thickness of the lithospheric plate (e.g. Smirnov & Sugrobov 1979, 1980a,b) (Fig. 1), as expected from the seismicity (Gorbatov *et al.* 1997). These observations seem to imply that the old Pacific Plate is now rejuvenated at the present position of Meiji Guyot. This implication has motivated us to perform tomographic inversion of *P*-wave traveltimes by adding regional reports to global data.

DATA AND METHOD

In order to achieve high resolution, the reports from 204 seismic stations of the Geophysical Survey of Russia (GSR) 1955–1997 were added to the catalogues of International Seismological Centre (ISC) 1964–1994 and USGS National Earthquake Information Centre (NEIC) 1995–1998. The recompiled data were reprocessed. The initial earth velocity model ak135 (Kennett *et al.* 1995) was perturbed by 10 per cent in the crust and 2 per cent in the mantle and hypocentral parameters of earthquakes were redetermined. Events with epicentral mislocation greater than 25 km were removed from the data set. The events not

* Now at: Research School of Earth Sciences, The Australian National University, Canberra ACT 0200, Australia
† Now at: Institut Teknologi Bandung, Jl. Ganesa 10, Bandung 40132, Indonesia

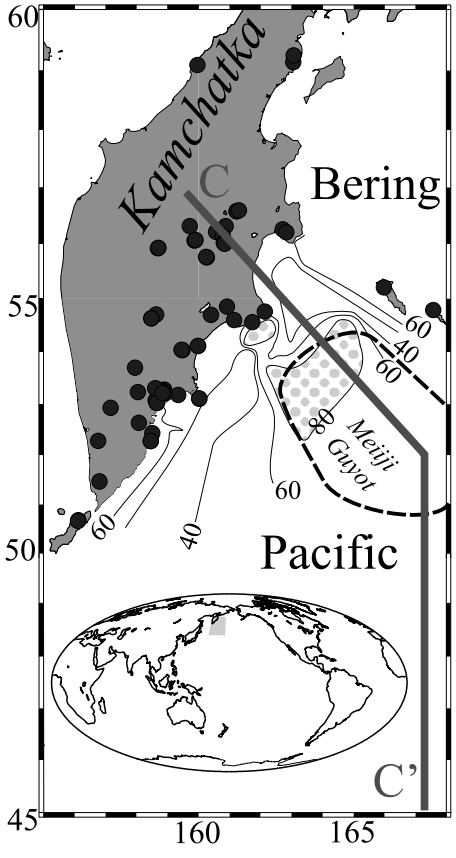

Figure 1. Map of the study region. Insert shows the location of the region as a shaded square in the North pacific. Thick black dashed line marks the approximate location of the Meiji Guyot seamount. Isocontours show the values of the heat flow measurements in mW m^{-2} recompiled from Selivestrov (1998). Isocontours on the Pacific seafloor are drawn only where the data are available. The grey dotted areas are those with anomalously high values of heat flow (higher 80 mW m^{-2}) (Selivestrov 1998). Solid black circles are the seismic stations of the Geophysical Survey of Russia located in the region under study. Solid line marked by CC′ shows the location of the cross-section presented in Fig. 3.

reported in the catalogue of Engdahl *et al.* (1998) were relocated using the ak135 earth model. For the other events, we did not attempt relocation but adopted the hypocentral parameters obtained by Engdahl *et al.* (1998) because of their extensive reprocessing procedure using *P*, *S*, *PKiKP*, *PKPdf* and the teleseismic depth phases *pP*, *pwP*, and *sP*. All the data were corrected for the Earth's ellipticity and station elevations. The study region is defined by a box with corners at 110°E, 75°N and 180°E, 30°N and depths of 0 and 1600 km. We used individual ray path data for the events occurring in the study region. For the events occurring outside, we constructed summary rays to reduce computation time, following the work of Widiyantoro & van der Hilst (1996). We combined ray paths from events in a $1^\circ \times 1^\circ \times 50$ volume to stations in a $1^\circ \times 1^\circ$ region into a single summary ray path. The residual time assigned to a summary ray was the median of all the data selected for that summary ray. Only ray paths with residuals less than 5 s and distances less than 95° were used. Each summary ray was composed of at least three individual rays. The study region was parametrized by cells of $1^\circ \times 1^\circ$ and 19 layers and the remaining whole Earth mantle by $5^\circ \times 5^\circ$cells and 16 layers.

The *P*-wave traveltime delays of a total of 934 957 ray paths were inverted for both the regional and global structures simultaneously to minimize contamination of our regional model by heterogeneities located outside. A 3-D ray tracing technique based on the 'pseudo-bending' method (Um & Thurber 1987), extended to a spherical earth by Koketsu & Sekine (1998), was used to generate data kernels. This inversion technique was presented in detail by Gorbatov *et al.* (2000) and Widiyantoro *et al.* (2000). The LSQR algorithm (Page & Saunders 1982) was used to solve a large and sparse system of equations. One iteration consists of the data kernel generation procedure and subsequent solution by LSQR. The ak135 earth model (Kennett *et al.* 1995) was adopted as the initial earth model for the first iteration. The velocity structure and hypocentral parameters were solved simultaneously in each iteration. Three iterations were performed, taking the resulting velocity model as the initial one for the subsequent iteration. The residual standard deviation was 1.42 s before the inversion, which decreased to 1.12, 0.94 and 0.93 s after the first, second and third iterations, respectively. We regarded the solution after the third iteration as the final one, in part because the 3-D ray tracing was time-consuming. It took about nine days for one iteration on a SUN Ultra 10 computer. The resolution matrix is difficult, if not impossible, to derive explicitly due to the method of solving the equation (Nakanishi & Suetsugi 1986; Inoue *et al.* 1990; Yao *et al.* 1999). Therefore, a checkerboard resolution test (Humphreys & Clayton 1988) was applied in order to analyse the sensitivity of tomographic solution. A checkerboard 3-D velocity structure was created in the study region. Negative and positive perturbations of 3 per cent were assigned to rectangular blocks. A pair of these blocks was separated by an unperturbed block in order to investigate the smearing effect of the resultant tomographic image. Three different block sizes, $2^\circ \times 2^\circ$, $3^\circ \times 3^\circ$ and $4^\circ \times 4^\circ$, were tested. The velocity perturbations obtained from the third iteration of the real data inversion were used as the structure in the outside region. This input structural model was used to generate a synthetic data set, to which random errors with a standard deviation of 1 s were added in order to simulate the errors contained in the real data set. The resultant synthetic data set was inverted to examine how the original velocity perturbation model was recovered.

We performed an additional test known as the 'restore resolution test' to examine to what extent a continuous structure in the tomographic image is a resolvable feature. In the present study we are interested in the vertically continuous structure that may represent a mantle plume. We therefore generate a hypothetical vertical structure similar to the one obtained from the real inversion but consisting of a blockwise succession of anomaly rather than a smooth continuation. If this block by block succession was recovered from inversion of the synthetic data, the continuity of the structure may be assured on a scale of the block size (e.g. Bijwaard *et al.* 1998).

SEISMIC IMAGE OF THE MANTLE PLUME

Fig. 2 is a part of the result, showing a prominent low-velocity anomaly underneath the Pacific Plate, with a perturbation of the order of −2 per cent on its axis relative to the ak135 earth model. This cylindrical anomaly has its bottom slightly below ∼900 km depth, not significantly deeper than 1000 km. Its horizontal image has maximum diameters (in plan view) of ∼500

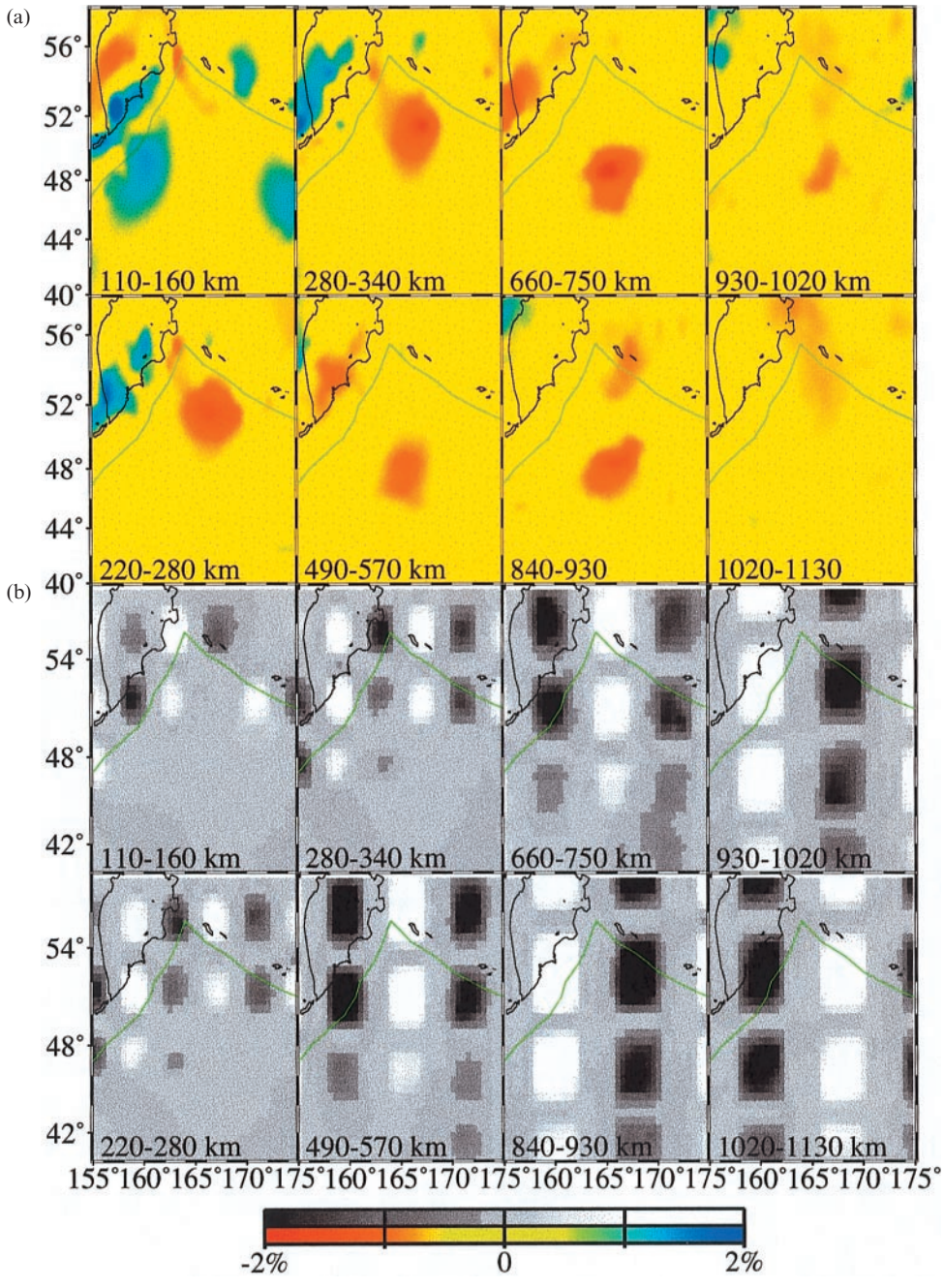

Figure 2. Eight representative layers of the tomographic images in the study region (a) and corresponding layers with checkerboard resolution tests (b). The velocity perturbation scale (per cent) relative to the ak135 earth model (Kennett *et al.* 1995) is shown at the bottom.

and ~300 km in the N–S and E–W directions, respectively, with its centre roughly at ~167°E, ~46°N. Although this is certainly a blurred image, it would be difficult to detect a plume conduit, if any, by our technique if its diameter were as small as ~100–200 km as suggested by e.g. Ribe & Christensen (1994) and Nataf (2000). The column of the anomaly is almost vertical up to depths of ~400 km, above which it rises obliquely to the north so that its horizontal cross-section is centred roughly at ~167°E, ~52°N at a depth of ~200 km. The northern half of this cross-section corresponds geographically to the southern half of Meiji Guyot. The structure of the low-velocity column at shallowest depths is poorly constrained. At depths above ~300 km a subsidiary anomaly extends subhorizontally to the NW direction along the trend of Meiji Guyot at the northern end of the Emperor seamounts. Although this feature can be traced upwards to depths as shallow as ~100 km, it is not well constrained at depths above ~200 km (Fig. 2). Thus, the low-velocity column consists of three parts, the lower part extending vertically through depths of ~900 to ~400 km, the upper part rising obliquely to the north up to ~200 km depth, and the subsidiary part extending subhorizontally to the NW at depths above ~300 km.

Fig. 3 shows the composite cross-section along the N–S and NW–SE profiles as indicated in Fig. 1. This composite cross-section shows a clear image of the mantle plume originating in the lower mantle, rising vertically through the transition

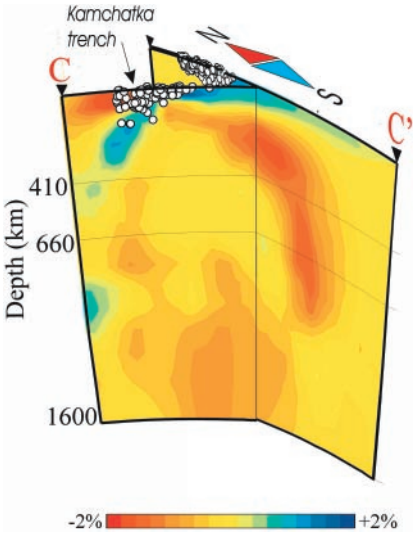

Figure 3. Cross-section of the tomographic model (see Fig. 1 for location). The velocity perturbation scale (per cent) relative to the ak135 earth model (Kennett *et al.* 1995) is shown at the bottom.

zone and then rising obliquely, with a subsidiary subhorizontal extension under the moving surface plate. Because of the limited resolution it is difficult at present to discuss in detail the plume configuration for depths shallower than 200 km (Fig. 2). We note, at the same time, that the surface plate has been mapped as a fast anomaly at the top of the mantle in the relevant region. As shown in Fig. 3, this plate anomaly is connected westwards to the subducted slab image and the underlying plume image is connected to the downgoing low velocity zone subparallel to the subducted slab image. The downgoing low-velocity zone continued from the rising plume image rolls backward at depths of $\sim$800 km, giving an image of a rolling cell of convection. However, such an image is likely to be an artefact of drawing at very limited location of cross-section, as indicated in Fig. 2 where the NE–SW trending low-velocity anomaly in depth range 280–750 km along the Kamchatka arc is spatially separated from the N–S trending low-velocity anomaly in a depth range 930–1130 km at the western end of the Aleutian arc.

Fig. 2(b) shows a part of the results of the checkerboard resolution tests, indicating that the resolution is, in general, better (i.e. the pattern is more clearly visible) at greater depths and further north. Bearing this tendency in mind, the mantle plume image is a resolvable feature in checkerboards with a length scale of 200–400 km and at depths below 160 km. In particular, the plume image extends downwards to a depth of $\sim$900 km but not beyond $\sim$1000 km. Its shallowest feature in the uppermost mantle is poorly resolved. The shallow NW-trending low-velocity anomaly is a resolvable feature in two layers at depths 160–340 km but not in the layer above at depths of 110–160 km. In Fig. 3, therefore, the configuration of the plume image in the uppermost mantle still remains uncertain. At greater depths the vertically continuous column is a resolvable feature on a vertical scale of $\sim$100 km, as the result of the restore resolution test in Fig. 4 demonstrates.

DISCUSSION

Mantle plumes rising from sources deep in the mantle have rarely been observed directly. Exceptions include the mantle plumes beneath Iceland (Wolfe *et al.* 1997; Shen *et al.* 1998;

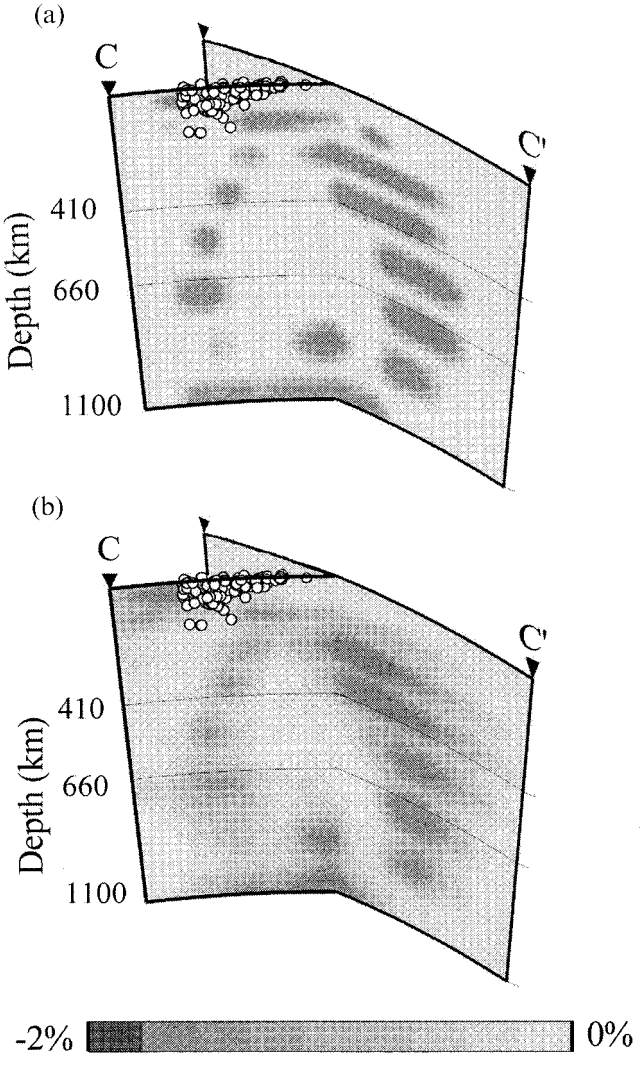

Figure 4. Result of the restore resolution test. (a) Synthetic input model. The hypothetical mantle plume is stripped by zero perturbations in odd numbered layers. (b) Recovered synthetic model. Location of cross-section is the same as in the Fig. 3. The velocity perturbation scale (per cent) relative to the ak135 earth model (Kennett *et al.* 1995) is shown at the bottom.

Bijwaard *et al.* 1998; Bijwaard & Spakman 1999), Africa (Ritsema *et al.* 1999), central Europe (Goes *et al.* 1999), and a possible fossil plume beneath Brazil (VanDecar *et al.* 1995). These studies, however, did not indicate at which depth a plume originates or how it interacts with the surface plate. We, for the first time, report evidence of a mantle plume originating near 1000 km depth, rising through the transition region across the 660 km discontinuity, bending obliquely near the top of the transition region and reaching upwards to at least 200 km depth. The lithospheric plate has been imaged as the high-velocity anomaly that continues northwestwards to the high-velocity anomaly associated with the slab subducting beneath Kamchatka. A part of the rising plume image deflects at depths above $\sim$300 km in the NW direction in fair agreement with the direction of movement the Pacific plate, suggesting that the plume conduit is deflected by the mantle shear flow due to the lithospheric plate motion (see e.g. Duncan & Richards (1991) for references). As demonstrated in the experiment of Richards & Griffiths (1988), the plume trajectory depends on the plume

size, the viscosity distribution and flow pattern in the mantle. According to their study, the subhorizontal deflection of the plume conduit at depths above ~300 km may be diagnostic of a large viscosity contrast across this depth. Similarly, the vertical rise of the plume from ~900 to ~400 km depth may suggest both a high viscosity and low influence of mantle return flow in this depth range, at least in this particular region.

The shallow (above ~300 km) subhorizontal portion of the mantle plume lies beneath Meiji Guyot. Meiji Guyot is an old seamount for which a minimum age of 61.9+5 Ma was estimated from the K–Ar dating of altered basalts at DSDP site 192 (Creager *et al.* 1973). The oldest overlying sediments were of early Maestrichtian age (Worsley 1973) so that the crust beneath Meiji Guyot must be at least 74.5 Ma or older (Mammerickx & Sharman 1988). According to Renkin & Sclater (1988), Meiji Guyot is located on the younger side of the 100 Ma isochron of the ocean floor and the Emperor seamounts to the south are on the older side without any age unconformity.

In contrast, distinct differences in bathymetry and gravity exist between Meiji Guyot and the Emperor seamounts to the south, as illustrated in Fig. 5. To the south of Meiji Guyot, both the topographic depression and negative free-air anomaly at the flank of the seamount progressively increase with increasing latitude, as expected from the progressive increase of seamount age (Jackson *et al.* 1972) and progressive decrease of seafloor age (Renkin & Sclater 1988; Lonsdale 1988; Rea *et al.* 1993), both of which contribute to the northward decrease of effective elastic thickness of lithosphere (Watts & Ribe 1984). Despite this expectation, no significant depression or negative gravity anomaly is associated with Meiji Guyot. Although this may be due in part to the much greater width of Meiji Guyot compared to that of other seamounts and in part to noise contamination of sediment and outer rise (lithospheric flexural upheaval) origins (Mammerickx & Sharman 1988), features of Meiji Guyot that may also be regarded as anomalous .

The ocean floor of Meiji Guyot is also marked by anomalously high heat flow, which could be considered as the most direct evidence for the presence of underlying mantle plume. Fig. 1 shows the oceanic heat flow distribution in Kamchatka, as compiled by Smirnov & Sugrobov (1979, 1980a,b) and Smirnov *et al.* (1992). Smirnov & Sugrobov (1979, 1980a,b) observed unusually high heat flow (higher than 80 mW m^{-2}) in the Meiji Guyot region and they suggested that the thermal thickness of the underlying plate is two–three times less than expected from normal oceanic plate of corresponding age. The reduced thermal thickness of the Pacific Plate upon its subduction into the northernmost part of the Kamchatka Trench has also been suggested from the maximum depth and dip angle of the Wadati–Benioff zone (Gorbatov *et al.* 1997). Although the subduction of bathymetric features is known to alter the seismic regime in a subduction zone (e.g. Vogt *et. al.* 1976; Chung & Kanamori 1978), a remarkable coincidence in the estimate of thermally reduced thickness of the Pacific Plate between its subducted portion and the portion left on the Earth's surface indicates that the plate in the region is in fact thermally younger.

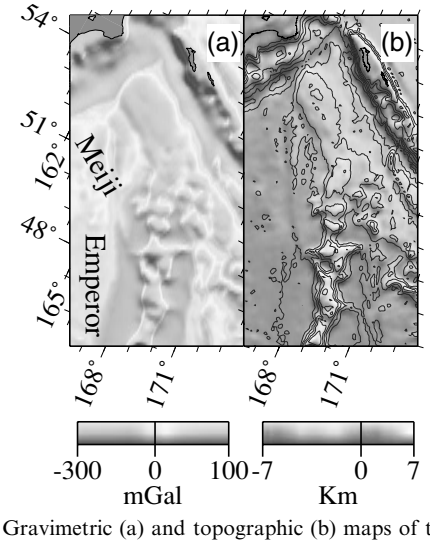

Figure 5. Gravimetric (a) and topographic (b) maps of the Emperor seamount chain (Smith & Sandwell 1995; Sandwell & Smith 1999). The 'Meiji' & 'Emperor' legends mark the Meiji Guyot & seamounts further to the south, respectively.

The upwelling hotter material of the plume would soften the lowermost part of the lithosphere, which could be removed by lateral shear stresses produced by horizontal flow in the asthenosphere (Davies 1995). Such removal would enhance the conduction of heat into the overlying lithosphere and be observed as anomalously high heat flow on the ocean floor of Meiji Guyot. Conversion of velocity perturbations into thermal anomalies, using the temperature derivatives of Nataf & Ricard (1996), shows that the temperature of upwelling plume is about 220 K higher than that of the surrounding 'normal' mantle. However, this value gives just a rough estimate, because traveltime tomography is not a very reliable source for such calculations (Nataf 2000). The heat flow anomaly associated with the thermal rejuvenation of lithosphere has been observed for a few hotspots (e.g. Courtney & White 1986; Detrick *et al.* 1986; Bonneville *et al.* 1997). The buoyant material of the plume would uplift the surface plate and would make the flexural signal of lithosphere insignificant if the area affected by the seamount loading is as broad as the area lifted by the plume, as may be the case of Meiji Guyot. A quantitative discussion, however, requires assessment of the effects of the sediment and outer rise on the topographic and bathymetric features of Meiji Guyot.

The source depth of this plume coincides roughly with the maximum penetration depth (~900 km) of the subducted Pacific slab below the Kamchatka peninsula and Kurile islands (e.g. Van der Hilst *et al.* 1991; Gorbatov *et al.* 2000; Fukao *et al.* 2000) and with the depth of the mid-mantle discontinuity (Kawakatsu & Niu 1994; Niu & Kawakatsu 1997; Vinnik *et al.* 1998). These coincidences may suggest some geophysical significance of the transition region across the 660 km discontinuity with its lower boundary near ~1000 km depth (e.g. Fukao *et al.* 2000).

CONCLUSIONS

Our non-linear tomographic inversion of traveltime data has revealed a mantle plume originating near ~900 km, rising across the 660 km discontinuity, tilting obliquely at the top of the transition zone, and in part extending subhorizontally with the moving lithospheric plate above. The bottom of this plume occurs between 900 and 1000 km. The top lies above 200 km depth but its structure is poorly resolved. The shallow portion of the mantle plume is located beneath Meiji Guyot, just oceanwards of the junction between the Aleutian and

Kamchatka trenches. The seafloor of Meiji Guyot is characterized by anomalously high heat flow and by the near absence of a gravity low on the flanks of this seamount. The thermal thickness of the subducted slab beneath northern Kamchatka has been estimated to be anomalously thin. We interpret these features as the surface manifestation of the process of thermo-mechanical erosion of the lithosphere by the mantle plume (Davies 1995). Unfortunately the resolution of tomography at depths where this process should occur is poor. Long-term ocean bottom seismic observations would improve this situation significantly.

ACKNOWLEDGMENTS

We thank B. L. N. Kennett, M. Obayashi and N. I. Selivestrov for useful suggestions and discussions. This manuscript benefited from constructive review by R. D. van der Hilst, S. Chevrot and an anonymous reviewer. We are also grateful to the staff members of the Geophysical Survey of Russia who helped us in data recompilation and digitization. AG and SW wish to thank JSPS for a postdoctoral fellowship to conduct research at the Earthquake Research Institute, University of Tokyo. The GMT software package of Wessel & Smith (1995) was used in our study.

REFERENCES

Bijwaard, H. & Spakman, W., 1999. Tomographic evidence for a narrow whole mantle plume below Iceland, *Earth planet. Sci. Lett.,* **166,** 121–126.

Bijwaard, H., Spakman, W. & Engdahl, E.R., 1998. Closing the gap between regional and global traveltime tomography, *J. geophys. Res.,* **103,** 30 055–30 078.

Bonneville, A., Von Herzen, R.P. & Lucazeau, F., 1997. Heat flow over Reunion hot spot track: additional evidence for thermal rejuvenation of oceanic lithosphere, *J. geophys. Res.,* **102,** 22 731–22 747.

Chung, W.Y. & Kanamori, H., 1978. Tectonic anomalies in aseismic ridge subduction in the New Hebrides arc, *Tectonophysics,* **50,** 29–40.

Courtney, R.C. & White, R.S., 1986. Anomalous heat flow and geoid across the Cape Verde Rise: evidence for dynamic support from a thermal plume in the mantle, *Geophys. J. R. astr. Soc.,* **87,** 815–867.

Creager, J.S. *et al.*, 1973. *Init. Rept. DSDP,* Vol. 19., US Govt Printng, Office, Washington, DC.

Davies, G.F., 1995. Penetration of plates and plumes through the mantle transition zone, *Earth planet. Sci. Lett.,* **133,** 507–516.

Detrick, R.S., Herzen, R.P.V., Parsons, B., Sandwell, D. & Dougherty, M., 1986. Heat flow observations on the Bermuda Rise and thermal models of midplate swells, *J. geophys. Res.,* **91,** 3701–3723.

Duncan, R.A. & Richards, M.A., 1991. Hotspots, mantle plumes, flood basalts, and true polar wander, *Rev. Geophys.,* **29,** 31–50.

Engdahl, E.R., van der Hilst, R.D. & Buland, R.P., 1998. Global teleseismic earthquake relocation with improved travel times and procedures for depth determination, *Bull. seism. Soc. Am.,* **88,** 722–743.

Fukao, Y., Widiyantoro, S. & Obayashi, M., 2000. Stagnant slabs in Bullen's transition region, *Rev. Geophys.,* in press.

Goes, S., Spakman, W. & Bijwaard, H., 1999. A lower mantle source for central European volcanism, *Science,* **286,** 1928–1931.

Gorbatov, A., Kostoglodov, V., Suarez, G. & Gordeev, E., 1997. Seismicity and structure of the Kamchatka subduction zone, *J. geophys. Res.,* **102,** 17 883–17 898.

Gorbatov, A., Widiyantoro, S., Fukao, Y. & Gordeev, E., 2000. Signature of remnant slabs in the North Pacific from *P*-wave tomography, *Geophys. J. Int.,* **142,** 27–36.

Humphreys, E. & Clayton, R.W., 1988. Adaptation of back projection tomography to seismic travel time problems, *J. geophys. Res.,* **93,** 1073–1085.

Inoue, H., Fukao, Y., Tanabe, K. & Ogata, Y., 1990. Whole mantle P-wave travel time tomography, *Phys. Earth. planet. Inter.,* **59,** 294–328.

Jackson, E.D., Silver, E.A. & Dalrymple, G.B., 1972. Hawaiian-Emperor Chain and its relation to Cenozoic circum-Pacific tectonics, *Geol. Soc. Am. Bull.,* **83,** 601–618.

Kawakatsu, H. & Niu, F., 1994. Seismic evidence for a 920-km discontinuity in the mantle, *Nature,* **6495,** 301–305.

Kennett, B.L.N., Engdahl, E.R. & Buland, R., 1995. Constraints on seismic velocities in the Earth from traveltimes, *Geophys. J. Int.,* **122,** 108–124.

Koketsu, K. & Sekine, S., 1998. Pseudo-bending method for three-dimensional seismic ray tracing in a spherical earth with discontinuities, *Geophys. J. Int.,* **132,** 339–346.

Lonsdale, P., 1988. Palaeogene history of the Kula plate: offshore evidence and onshore implications, *Geol. Soc. Am. Bull.,* **100,** 733–754.

Mammerickx, J. & Sharman, G.F., 1988. Tectonic evolution of the North Pacific during the Cretaceous quiet period, *J. geophys. Res.,* **93,** 3009–3024.

Nakanishi, I. & Suetsugi, D., 1986. Resolution matrix calculated by a tomographic inversion method, *J. Phys. Earth,* **34,** 95–99.

Nataf, H.-C., 2000. Seismic imaging of mantle plumes, *Ann. Rev. Earth. planet. Sci.,* **28,** 391–417.

Nataf, H.-C. & Ricard, Y., 1996. 3SMAC: an *a priori* tomographic model of the upper mantle based on geophysical modelling, *Phys. Earth planet. Int.,* **95,** 101–122.

Niu, F. & Kawakatsu, H., 1997. Depth variation of the mid-mantle seismic discontinuity, *Geophys. Res. Lett.,* **24,** 429–432.

Page, C.C. & Saunders, M.A., 1982. LSQR: An algorithm for sparse linear equations and sparse least squares, *ACM Trans. Math. Soft.,* **8,** 43–71.

Rea, D. *et al.*, 1993. Palaeoceanographic record of north Pacific quantified, *EOS, Trans. Am. geophys. Un.,* **74,** 406–411.

Renkin, M.L. & Sclater, J.G., 1988. Depth and age in the North Pacific, *J. geophys. Res.,* **93,** 2919–2935.

Ribe, N.M. & Christensen, U.R., 1994. Three-dimensional modelling of plume–lithosphere interaction, *J. geophys. Res.,* **99,** 669–682.

Richards, M.A. & Griffiths, R.W., 1988. Deflection of plumes by mantle shear flow: experimental results and a simple theory, *Geophys. J.,* **94,** 367–376.

Ritsema, J., van Heijst, H.J. & Woodhouse, J.H., 1999. Complex shear wave velocity structure imaged beneath Africa and Iceland. *Science,* **286,** 1925–1928.

Sandwell, D.T. & Smith, W.H.F., 1999. *Gravity Anomaly from Geosat and ERS-1 Altimetry, Versions 1–7, 1992–95,* SIO Geological Data Center, Pasedena (digital file available from www.jpl.nasa.gov/applications/data.html).

Shen, Y., Solomon, S.C., Bjarnason, I.Th. & Wolfe, S., 1998. Seismic evidence for a lower-mantle origin of the Iceland plume, *Nature,* **395,** 62–65.

Selivestrov, N.I., 1998. Structure of the oceanic floor near Kamchatka and the geodynamics of the zone of Kurile–Kamchatka and Aleutians trenches Joint. Nauchni Mir, Moscow (in Russian).

Smirnov, Y.B. & Sugrobov, V.M., 1979. Terrestrial heat flow in the Kurile-Kamchatka & Aleutian provinces—I, Heat flow and tectonics, *Volcanol. Seismol.,* **1,** 59–73 (in Russian).

Smirnov, Y.B. & Sugrobov, V.M., 1980a. Terrestrial heat flow in the Kurile-Kamchatka & Aleutian provinces—II, The map of measured and background heat flow, *Volcanol. Seismol.,* **1,** 16–31 (in Russian).

Smirnov, Y.B. & Sugrobov, V.M., 1980b. Terrestrial heat flow in the Kurile-Kamchatka and Aleutian provinces—III, Assessment of temperature at depth and thickness of the lithosphere (in Russian), *Volcanol. Seismol.,* **2,** 3–18.

Smirnov, Y.B., Sugrobov, V.M. & Yanovskiy, F.A., 1992. The terrestrial heat flow of Kamchatka, *Volcanol. Seismol.,* **13,** 181–210.

Smith, W.H.F. & Sandwell, D.T., 1995. Marine gravity field from declassified Geosat and ERS-1 altimetry, *EOS, Trans. Am. geophys. Un.,* **76,** Fall Mtng Suppl, F156.

Um, J. & Thurber, C., 1987. A fast algorithm for two-point seismic ray tracing, *Bull. seism. Soc. Am.,* **77,** 972–986.

Van der Hilst, R.D., Engdahl, R., Spakman, W. & Nolet, G., 1991. Tomographic imaging of subducted lithosphere below northwest Pacific island arcs, *Nature,* **353,** 37–42.

VanDecar, J.C., James, D. & Assumpção, M., 1995. Seismic evidence for a fossil mantle plume beneath South America & implications for plate driving forces, *Nature,* **378,** 25–31.

Vinnik, L., Niu, F. & Kawakatsu, H., 1988. Broadband converted phases from midmantle discontinuities, *Earth Planets Space,* **50,** 987–997.

Vogt, P.R. *et al.*, 1976. Subduction of aseismic ridges: Effects on shape, seismicity & other characteristics of consuming plate boundaries *Geol. Soc. Am. Spec. Pap.,* **172,** 59.

Watts, A.B. & Ribe, N.M., 1984. On geoid heights and flexure of the lithosphere at seamounts, *J. geophys. Res.,* **89,** 11 152–11 170.

Wessel, P. & Smith, W.H.F., 1995. New version, of the Generic Mapping Tools released, *EOS, Trans. Am. geophys. Un.,* **76,** 329.

Widiyantoro, S. & van der Hilst, R.D., 1996. Structure and evolution of the lithospheric slab beneath Sunda arc, Indonesia, *Science,* **271,** 1566–1570.

Widiyantoro, S., Gorbatov, A., Kennett, B.L.N. & Fukao, Y., 2000. Improving global shear wave traveltime tomography using three-dimensional ray tracing and iterative inversion, *Geophys. J. Int.,* **141,** 747–758.

Wolfe, C.J., Bjaranson, I.Th., VanDecar, J.C. & Solomon, S., 1997. Seismic structure of the Iceland mantle plume, *Nature,* **385,** 245–247.

Worsley, J.R., 1973. Calcareous nanno-fossils, leg 19 of the Deep Sea Drilling Project, *Init. Rept DSDP.,* **19,** 741–750.

Yao, Z.S., Roberts, R.G. & Tryggvason, A., 1999. Calculating resolution and covariance matrices for seismic tomography with the LSQR method, *Geophys. J. Int.,* **138,** 886–894.